Immersed acoustic black hole as a travelling wave absorber: understanding artificial cochlear mechanics

Simon Foucaud, Guilhem Michon, Yves Gourinat, Adrien Pelat, François Gautier

ACOUSTICS 2012

Immersed acoustic black hole as a travelling wave absorber: understanding artificial cochlear mechanics

S. Foucaud[a], G. Michon[a], Y. Gourinat[a], A. Pelat[b] and F. Gautier[b]

[a]Université de Toulouse - ICA - ISAE, 10 av. Edouard Belin, 31055 Toulouse, France
[b]Laboratoire d'acoustique de l'université du Maine, Bât. IAM - UFR Sciences Avenue Olivier Messiaen 72085 Le Mans Cedex 9
guilhem.michon@isae.fr

Inner ear is constituted of fluid-filled ducts partitioned with an elastic structure, the organ of Corti. When the inner ear is excited by sound, travelling waves appear along the organ of Corti and stimulate the sensory cells. A peak of vibration is reached at a particular place depending on the excitation frequency. The waves are strongly attenuated after this place. Due to the complexity of *in vivo* experimentations, some aspects of physiological functions still need to be investigated.
For this purpose, an experimental setup reproducing the passive behavior of the inner ear has been designed and manufactured. Standing waves are usually observed on artificial cochlea devices due to wave reflection on boundaries. Acoustic black holes are known as vibration absorbers for thin structures. In this paper, an immersed acoustic black hole is used to reduce the reflected wave. The impedance matrix method is used to estimate the reflection coefficient of the acoustic black hole. Travelling waves are observed and this device allows better understanding of artificial cochlear mechanics.

1 Introduction

The inner ear plays a major role for pilot's perception and orientation. Consequently its global modeling is a great challenge. Previous studies focused on the modeling of the vestibular system [9] and the present paper deals with the understanding of the cochlea which is physically connected to the vestibular system. The mammalian organ of hearing is constituted of a fluid-filled duct partitioned with two membranes. The compliance of the basilar membrane varies along the cochlea. When it is acoustically stimulated the response localization is frequency dependent. A wave travels from the base to the apex of the cochlea with peak of maximum amplitude at a particular place. This frequency-place relation allows sound discrimination. The organ of Corti stands on the basilar membrane and plays the role of sensing the vibration and amplifying it. Artificial cochlea is the name given to the devices reproducing the mechanical behavior of the mammalian basilar membrane. Filtering mechanical vibrations and converting them in electrical field without the help of a power-consuming processing device is a very promising future for artificial cochleas.
As the longitudinal mechanical coupling seems to be very low, the mammalian basilar membrane is often represented in literature with local mechanical impedance [11, 8]. Plate [10] or membrane [12] models are classically used for the representation of artificial cochleas. Most of artificial cochleas are passive as no feedback elements are added [13, 14]. Vibrations are measured with the help of piezoelectric patches [10] or a laser velocimeter [10, 13, 14]. The frequency-place relation is observed but under the form of standing waves. In the inner ear, waves are attenuated before they reach the apex because of interstitial fluid viscosity and no reflection occurs [2]. This kind of mechanism is not easily reproducible even with micromachining techniques [13]. Interesting results can be obtained by increasing the fluid viscosity [12]. Here a new method is tested to observe traveling waves on an artificial metallic support. The Acoustic Black Hole (ABH) effect takes place for flexural waves propagating toward sharp edges [6, 4]. In the present paper, the ABH is used for the attenuation of the wave reflection.
This paper first briefly described the assumptions used in a classical model for an immersed width varying plate. Then the ABH principle is described and the impedance matrices model estimates the reflection coefficient of an ABH. Finally the experimental setup is presented combining both effect of varying width plate and ABH. Experimental results are exposed and compared to theoretical ones previously detailed in [3].

2 Mechanical model

2.1 Waveguide

Let consider a waveguide constituted by a rectangular fluid-filled ducts partitioned by a solid plate (see Figure (1)). The dynamic equation for an isotropic flexural plate is :

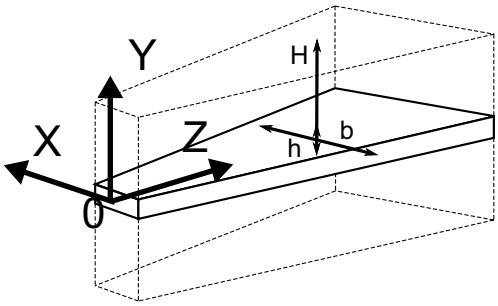

Figure 1: Box model of a varying width plate immersed between two symetric ducts.

$$D\left(\frac{\partial^4 W}{\partial z^4} + 2\frac{\partial^4 W}{\partial z^2 \partial x^2} + \frac{\partial^4 W}{\partial x^4}\right) + \rho_s h(z)\frac{\partial^2 W}{\partial t^2} = p_f \quad (1)$$

where W is the deflection of the plate, $h(z)$ the thickness, ρ_s the density, D the flexural rigidity defined by $D = Eh(z)^3/12(1-\nu^2)$ with E the Young modulus of the plate, ν the Poisson's ratio. p_f the fluid pressure applied on the plate. Assuming incompressibility and no viscosity, the fluid pressure p_f verifies the Laplace equation in the fluid domain:

$$\Delta p_f = 0 \quad (2)$$

The Wentzel-Kramers-Brillouin (WKB) method is used to solve this problem. This semi-analytic technique describes waveguides where the parameters are slowly varying along the direction of propagation. It gives a good approximation of the response with low computational costs. The application of the WKB method is adapted from Shintaku [10] and is more detailed in the previous paper [3].
First, the fluid pressure p_f is assumed as a sum of orthogonal modes:

$$p_f = -i\rho_f\omega \sum_{j=0}^{\infty} \cosh\left(\xi_j(y-H)\right) \sin\left(j\frac{2\pi}{b(z)}x\right) A_j(z) \mathrm{e}^{\int_0^z k(l)\mathrm{d}l} \mathrm{e}^{i\omega t} \quad (3)$$

with $\xi_j = \sqrt{k^2 + (2j\pi/b(z))^2}$, where $b(z)$ is the local width of the plate. Assuming a small variation of the magnitude term $A_j(z)$, the Laplace equation is verified. This expression also allows the pressure to verify the hard wall boundary conditions on ducts walls and the continuity of velocity field on

the fluid structure interface.
Deflection of the plate is also assumed under a waveform:

$$W(x,y,z,t) = s_t(x,y)W_e(z)\mathrm{e}^{\int_0^z k(l)\mathrm{d}l}\mathrm{e}^{i\omega t} \quad (4)$$

where $s_t(x,y)$ is the transversal assumed mode shape and $W_e(z)$ is the longitudinal envelope function. The dispersion relation is obtained through substituting the expressions Eq. (3) and Eq. (4) in Eq. (1). Admissible solutions for the wavenumber k are determined with the dispersion relation. Each solution k has its coupled solution $-k$ which means that two similar waves propagating in opposite directions are solutions of the system. The amplitude of vibration is obtained from the invariance of the time-averaged Lagrangian [11]:

$$\frac{\mathrm{d}}{\mathrm{d}z}\frac{\partial \mathcal{L}}{\partial k} = 0 \quad (5)$$

This method is not developed further here and the results are used later in the present paper.

2.2 Acoustic Black Hole

The theoretical approach considering only an incident wave is only valid in the case of an infinite waveguide. Practically, boundary conditions provide reflections of the incident propagating waves in reflected waves. Since they have the same wavenumber, the interferences between the incident and reflected waves provide standing waves. Here, the supported idea is to use an acoustic black hole as an anechoic end to the flexural plate. The aim is to reduce the amplitude of the reflected wave and thus to decrease the presence of standing waves.
The acoustic black hole consists of a power-law profile of thickness:

$$h(z) = \alpha(z_t - z)^2 \quad (6)$$

where $\alpha = h(z_0)/L_{ABH}$ is the ratio of the initial thickness at the abscissa z_0 to the total length of the ABH and z_t is the theoretical abscissa of the ABH's end. When the z position tends to z_t, the flexural wave number is increasing and tends theoretically to infinity. At the same time, the group speed tends to zero. This means that the propagation of the wave is stopped and it never reaches the end of the black hole. Thus, no wave is reflected. Practically, the edge is truncated and the ratio between the reflected and incident wave is never zero. A visco-elastic material layer (see Figure 2) is attached to the plate to keep this ratio as low as possible. The procedure of designing an acoustic black hole is detailed in [7, 1]. Georgiev & al. [5] described and studied analytically the acoustic black hole effect using the impedance matrix method. This method is used here to estimate the ABH efficiency. The reflection coefficient which corresponds to the ratio of the reflected wave amplitude to the incident wave amplitude is plotted on the Figure (3) using the parameters of Table 1. It is solved for the case of a beam not surrounded by fluid. Due to fluid mass and viscosity, it is assumed that this coefficient is lower in the case presented here.

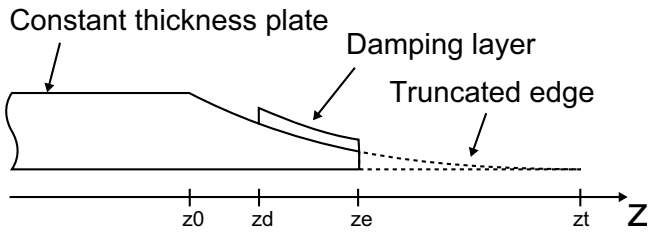

Figure 2: Truncated acoustic black hole with an visco-elastic damping layer.

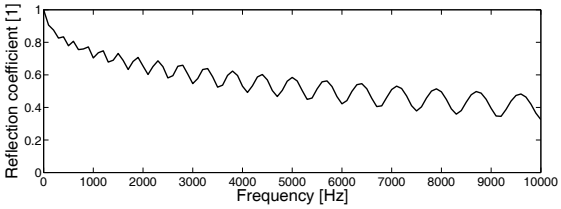

Figure 3: Reflection coefficient solved for a beam in the air with Georgiev method [6].

3 Experimental setup

3.1 Design

The acoustic black hole (ABH) efficiency is related to the length of the decreasing thickness zone [6, 1]. Due to the machining process, the initial thickness of the acoustic black hole is at least of 1mm. This constraint sets the tonotopic zone thickness. The longer the ABH is the more efficient it is. The accuracy of the machining process also decreases with the length. Finally, the length of the ABH is a compromise between the machining constraint and the efficiency, knowing the fact that the reflection coefficient can be additionnally reduced by a damping layer of visco-elastic material. The parameters of the tonotopic zone are chosen to obtain a frequency response between 0.3kHz and 3kHz when immersed in water. This frequency bandwidth is included in the human hearing range. The range is limited to avoid the second or higher order transverse mode to mix with the first mode. The model (see Section (2.1)) is used to determine the second transverse mode frequency response substituting the corresponding function $s_t(x,y)$ in the expression Eq. (4). The procedure briefly exposed in the Figure (4) gives a width of 0.03m at the narrow start of the plate and a width of 0.05m at the wide end. Since the plate is excited on the median segment (see Section 3.3), it is assumed that the first mode is mainly excited. Thus the dimensions are extended to fit with the bandwidth [0.3 − 3kHz]. The device is as long as permitted by the manufacturing means. The parameters are summarized in the following table (see Table 2):

Table 1: Acoustic black hole parameters

Parameter	Symbol	Value
Length of the ABH	L_{ABH}	375mm
Initial thickness	$h(z_0)$	1mm
Young's modulus	E	72000MPa
Measured residual thickness	$h(z_e)$	80μm

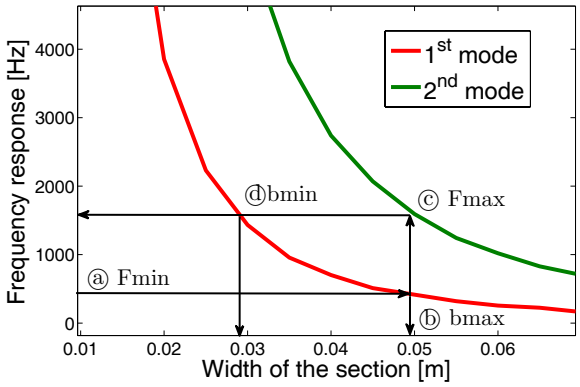

Figure 4: Procedure for choosing the dimensions of the varying width plate. Starting with the step ⓐ from the lower desired frequency *Fmin* the width *bmax* at which the first mode will respond is obtained at the step ⓑ . Then the step ⓒ with the same section, the frequency response *Fmax* of the second mode is determined. Finally at the step ⓓ the width *bmin* of the section responding with the first mode to the frequency *Fmax* is obtained.

Table 2: Tonotopic zone (TZ) parameters

Parameter	Symbol	Value
Length of the TZ	L_{tz}	375mm
Thickness	h_0	1mm
Width of the narrow end	*bmin*	22mm
Width of the wide end	*bmax*	60mm
Young's modulus	*E*	72000MPa

3.2 Manufacturing

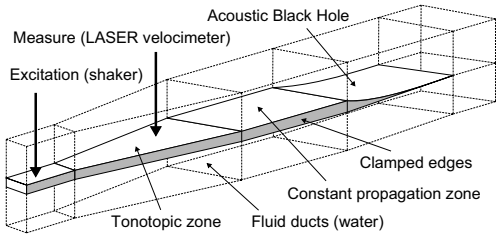

Figure 5: Descriptive diagram of the experimental setup.

The acoustic black hole and the varying width plate are machined in the same part (see Figure 5). The aluminum vibrating plate is clamped between two steel frames which also constitute ducts walls. The upper wall is a transparent Plexiglas® plate allowing velocity measurements. Most operations of manufacturing necessary are derived from standard operations. The tight point is the machining of the power-law decreasing thickness of the acoustic black hole. A good competence in machining is needed to realize this operation. The extension of these techniques to a life-sized artificial cochlea device still needs to be investigated.

3.3 Measurement

The observation of traveling waves on the device requires two more additional systems : the excitation and the measurements means. While the cochlea is excited with acoustic pressure coming through the stapes, the varying width plate is here excited through an electromagnetic shaker. As the plate is relatively stiff compared to the basilar membrane, the acoustic excitation required would be inconceivable. The varying width section is extended with a constant width section to allow the fastening of the shaker to the plate. A piezoelectric force sensor is inserted between the shaker and the plate to provide a reference. The response of the vibrating plate is measured with a scanning laser vibrometer. The laser beam is going perpendicularly to the plate and measure the velocity along the out-of-plane direction. This value is divided by the reference in order to obtain Frequency Response Functions (FRF). The input signal is a burst sine chirp

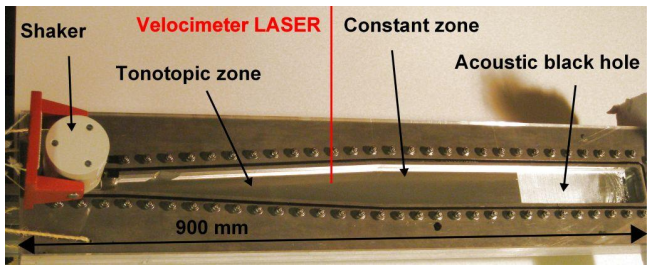

Figure 6: Annoted photography of the assembled experimental setup.

on the frequency bandwidth [0 – 10kHz]. Since 6400 frequency lines are used, the frequency resolution is close to 1.6Hz. The time duration of each acquisition is 1.28s and data of each point are averaged on six acquisitions for a better signal/noise ratio. The preliminary measurements on the whole surface of the plate has shown a first transversal mode dominance. Thus, the measurements are realized only on the median segment which reduces the number of points to be measured or increases the spatial resolution.

4 Results

The results are obtained through a series of FRF defined for the frequencies f_j and for the points of coordinates (x_i, z_i). The vector of frequencies $[f_j]$ is constituted by 6400 components equally distributed on the bandwidth [0 – 10kHz]. For each measured point $P(x_i, z_i)$, and each frequency f_j the FRF is given as a complex number $H(P(x_i, z_i), f_j)$. Complex values are needed for the study of travelling waves as the latter can be considered as complex modes. The entire data set consists of the terms $H(P(x_i, z_i), f_j)$ which are transformed hereafter for a better lisibility.

4.1 Data processing

Using the data for a particular frequency f_m and the whole set of points, the Operating Deflection Shape (ODS) is obtained by taking the real part of $H(P(x_i, z_i), f_m)$. This could also provides animated ODS, multiplying by a rotating term $e^{i\omega t}$. Animations are useful tools but the envelope functions are a better representation of the results. Envelope functions can be obtained by taking $|H(P(x_i, z_i), f_m)|$. An example is

given on Figure (7) for the frequency f_m = 5706Hz and for the points $P(0, z_i)$ located along the median segment of the plate. The general feature of the envelope curve is well cor-

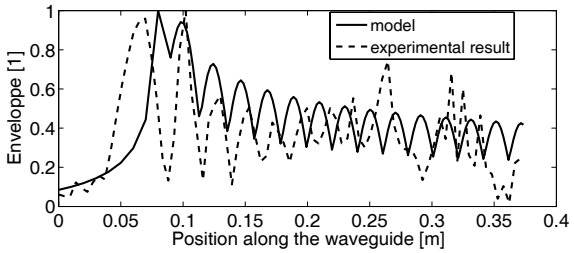

Figure 7: Envelope function of the plate immersed in the air, measured for f_m = 5706Hz.

related with the model (see Section 2.1) including a reflection coefficent $R = 0.3$. The higher peaks are located in the same area for model and experimental results. The decreasing amplitude of peaks after the shows the same trend as well. However, the peaks are not superposed and more comparative plots are needed. The unwrapped angle $\angle(H(P(0, z_i), f_m))$ is used in order to obtained the phase function of the travelling wave. The comparison between the model and the experimental results for the same frequency f_m is shown on the Figure (8). This curve shows three important features :

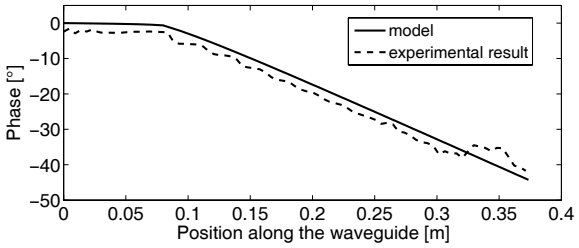

Figure 8: Phase function of the plate immersed in the air, measured for f_m = 5706Hz.

- The phase of vibration is varying and depends on the position along the waveguide. The ABH allows this result as total reflection would provide standing waves with a constant phase. Hence, travelling waves are observed.
- The position of the breakdown in the phase slope is easily observable at the same location for the model and the experimental results. This location corresponds to the location of the highest peak and it is related to the excitation frequency. The clear identification of this location proves that the experimental results are workable.
- The value of the slope itself is closed to the one from the model. It determines the wavelength after the peak and the number of secondary peaks.

These results are also found by using the wavenumber curves which are plotted on the Figure (9), taking the derivative of the previous phase curves along the position. A strong variation of the wavenumber is located at the abscissa corresponding to the peaks of amplitude and the phase breakdowns. Before this point, the wavenumber is close to zero which means an almost in-phase vibration. After this point, the

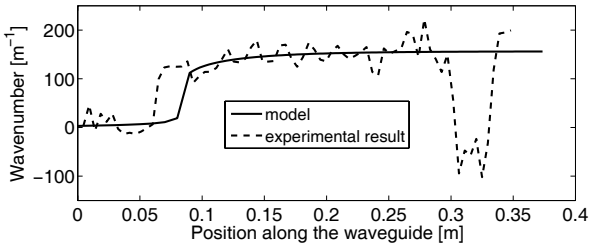

Figure 9: Wavenumber of the plate immersed in the air, measured for f_m = 5706Hz.

wavenumber reaches an asymptotic value which is the same for the model and the experimental results. As the derivative is very sensitive to the measurements noise, perturbations of the experimental curve is oscillating around this value. The three previous figures show that the experimental results are closed from the model at a given frequency. The frequency f_m = 5706Hz is arbitrary chosen but similar results are obtained for others frequencies.

4.2 Tonotopy

Since the objective of this study is to show a tonotopy on the varying width plate, these data are used to plot tonotopic maps. For each frequency, the envelope function (See Figure (7)) is normalized and plotted on a color map. The blue color corresponds to no vibration zones and the red color to the zones of maximum vibration. The relation between the frequency and the location of vibration clearly appears. A similar relation is also extracted from the model taking the location of the maximum response point for each frequency. Model and experimental results are compared on Figure (10) for the plate in the air and on Figure (11) for the plate immersed in water. For the case in the air, the experimental

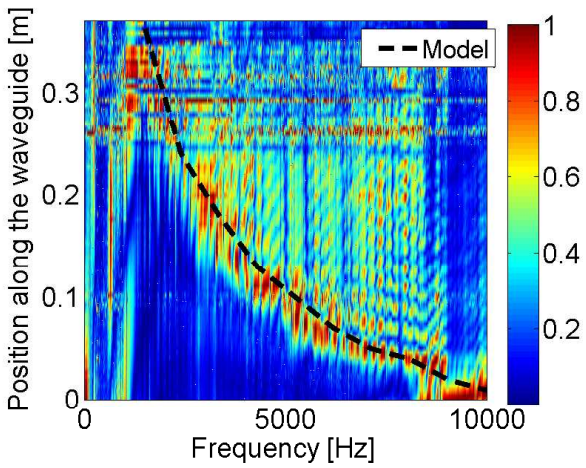

Figure 10: Experimental tonotopic map obtained by taking the normalized response for each frequency. Map for the plate immersed in the air.

results show a good correspondence with the model. The Zone of Maximum Vibration (ZMV), represented with the red color on Figure (10), is located around the dashed line corresponding to the model. The area under the ZMV is almost uniformly colored and the magnitude of vibration is close to zero. This makes the identification of the ZMV even clearer. The area above the ZMV presents some secondary

peaks but their magnitude is clearly smaller than in the ZMV, thanks to the effect of the ABH. For a vibration in a given location, the excitation frequency is identified which is the objective of this device. Horizontal lines appear for a location close from 0.3m. These are due to clamping defaults.

The tonotopic map for the plate immersed in water is plotted following the same method on Figure (11). The ZMV is shifted toward lower frequencies due to the inertia effect of water. The general form of the ZMV is identified. Above 2.5 kHz, the experimental results are comparable to the model. The secondary peaks are visible but significantly attenuated. For lower frequencies, due to interference of frame modes in the same frequency bandwidth, several peaks appear and the relation between location and frequency is not clearly visible. Modifications of the frame are under investigation in order to solve this problem.

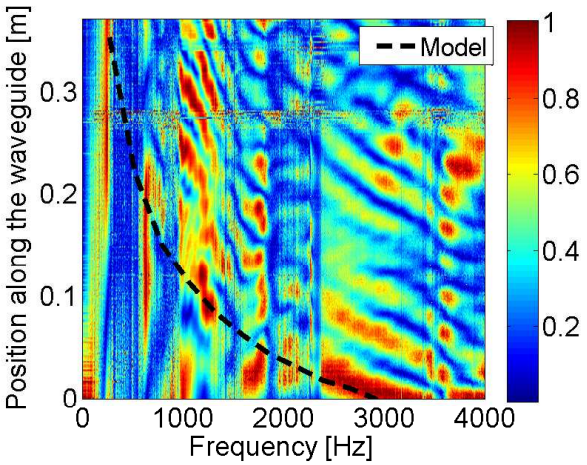

Figure 11: Experimental tonotopic map obtained by taking the normalized response for each frequency. Map for the plate immersed in water.

5 Conclusion

The device presented here allows the observation of travelling waves. Due to the variation of waveguide properties, the travelling waves show a peak of maximum amplitude. The provided relation between frequency and location of the maximum vibration peak is called the tonotopy. This concept allows sound frequency selectivity in the inner ear. The experimental results presented here show a good correlation with the model. The acoustic black hole used as an anechoic end improves the quality of measurements. The device allows a better understanding of inner ear mechanics and it lays the foundations of an acoustic sensor concept.
However some aspects of this study are still under investigation. The frame stabilization and the study of the immersed acoustic black hole will be the next steps of this work.

Acknowledgments

The author would like to acknowledge the staff of the Laboratoire d'Acoustique de l'Université du Maine (LAUM) where the experimental sessions took place and especially Stanislas Renard who machined the acoustic black hole.

References

[1] J. Cuenca. *Wave models for the flexural vibrations of thin plates*. PhD thesis, Université du Maine, Le Mans, France, 2009.

[2] E. De Boer and R. MacKay. Reflections on reflections. *The Journal of the Acoustical Society of America*, 67:882, 1980.

[3] S. Foucaud, G. Michon, Y. Gourinat, A. Pelat, and F. Gautier. Designing an experiment inspired by cochlea for travelling waves observation. In *Proceedings of the IMAC XXX, Jacksonville*, 2012.

[4] F. Gautier, J. Cuenca, V.V. Krylov, and L. Simon. Experimental investigation of the acoustic black hole effect for vibration damping in elliptical plates. *Acoustical Society of America Journal*, 123:3318, 2008.

[5] V. B. Georgiev, J. Cuenca, F. Gautier, and L. Simon. Vibration reduction of beams and plates using acoustic black hole effect. 2010.

[6] VB Georgiev, J. Cuenca, F. Gautier, L. Simon, and VV Krylov. Damping of structural vibrations in beams and elliptical plates using the acoustic black hole effect. *Journal of sound and vibration*, 330:2497–2508, 2011.

[7] VV Krylov and F. Tilman. Acoustic 'black holes' for flexural waves as effective vibration dampers. *Journal of Sound and Vibration*, 274(3-5):605–619, 2004.

[8] S. T. Neely and D. O. Kim. A model for active elements in cochlear biomechanics. *Journal of the Acoustical Society of America*, 79(5):1472–1480, 1986. Times Cited: 193.

[9] P. Selva, J. Morlier, and Y. Gourinat. Development of a dynamic virtual reality model of the inner ear sensory system as a learning and demonstrating tool. *Modelling and Simulation in Engineering*, 2009:5, 2009.

[10] H. Shintaku, T. Nakagawa, D. Kitagawa, H. Tanujaya, S. Kawano, and J. Ito. Development of piezoelectric acoustic sensor with frequency selectivity for artificial cochlea. *Sensors and Actuators A: Physical*, 158(2):183–192, 2010.

[11] C.R. Steele and L.A. Taber. Comparison of wkb calculations and experimental results for three-dimensional cochlear models. *The Journal of the Acoustical Society of America*, 65:1007, 1979.

[12] R.D. White. *Biomimetic trapped fluid microsystems for acoustic sensing*. PhD thesis, University of California, San Diego, 2005.

[13] R.D. White and K. Grosh. Microengineered hydromechanical cochlear model. *Proceedings of the National Academy of Sciences of the United States of America*, 102(5):1296, 2005.

[14] Gan Zhou, Louis Bintz, Dana Z. Anderson, and Kathryn E. Bright. A life-sized physical model of the human cochlea with optical holographic readout. *The Journal of the Acoustical Society of America*, 93(3):1516–1523, 1993.